A New Hand-Held Microsystem Architecture for Biological Analysis

Moisés Piedade, Leonel Augusto Sousa, *Senior Member, IEEE*, Teresa Mendes de Almeida, José Germano, Bertinho d'Andrade da Costa, João Miranda Lemos, Paulo Peixeiro Freitas, *Member, IEEE*, Hugo A. Ferreira, and Filipe Arroyo Cardoso

***Abstract*—This paper presents a hand-held microsystem based on new fully integrated magnetoresistive biochips for biomolecular recognition (DNA hybridization, antibody antigen interaction, etc.). Magnetoresistive chip surfaces are chemically treated, enabling the immobilization of probe biomolecules such as DNA or antibodies. Fluid handling is also integrated in the biochip. The proposed microsystem not only integrates the biochip, which is an array of 16×16 magnetoresistive sensors, but it also provides all the electronic circuitry for addressing and reading out each transducer. The proposed architecture and circuits were specifically designed for achieving a compact, programmable and portable microsystem. The microsystem also integrates a hand-held analyzer connected through a wireless channel. A prototype of the system was already developed and detection of magnetic nanoparticles was obtained. This indicates that the system may be used for magnetic label based bioassays.**

***Index Terms*—Biochip, biological analysis, microsystem, magnetoresistive sensor.**

I. Introduction

RECENTLY, there has been a continuously increasing research effort for developing highly integrated instruments, which are able to automatically deliver results concerning drug and antibiotic administration, DNA hybridization detection, etc., not only near the patient but also in real time. The main goal of this research is to obtain a complete lab-on-a-chip system for the highly demanding medical-diagnostic market. These instruments are frequently based on biochips, which are recent technological breakthroughs achieved by combining expertise of different research areas, such as biology, chemistry, microelectronics, signal processing, data mining, etc.

In some biochips designed for DNA recognition, DNA target is marked with a fluorescent molecule. The labelled target is then made to interact with DNA probes immobilized on the chip surface. DNA hybridization is detected by laser illumination of the biochip surface and by acquiring and processing the corresponding images. This type of biochip requires a bulky, sophisticated and expensive readout system, which does not facilitate the design of the envisaged modern hand-held instrument.

Recently, magnetoresistive biochips have been introduced for fully integrated biomolecular recognition assays [1], [2], using target biomolecules marked with magnetic particles. Subsequently, the labelled targets are recognized by biomolecular probes immobilized on the surface of the chip over sensing sites. The markers fringe magnetic fields are then detected by magnetic sensors [3]–[7]. The great advantage of this type of microsystem is the possibility to directly detect biomolecular recognition (eg. DNA hybridization) by reading the magnetic field created by the markers using a sensor located below each probe site. The action of taking an electrical measurement, instead of an optical one, reduces considerably the readout system complexity and increases sensitivity.

Among the various types of magnetic sensors, magnetic tunnel junctions (MTJs) assume greater importance because of their flexibility in resistance design (by changing the tunnel barrier thickness) and because they benefit from recent research and technological advances aiming at the design of future ultra high density magnetic memory chips [8]. This research already led to higher magnetic sensitivity, when compared with other types of magnetic sensors, which enables the detection of smaller magnetic labels.

In order to increase the number of magnetoresistive sensor sites in the biochip and make the biochip fully scalable, a new matrix-based magnetoresistive biochip was designed and fabricated. The biochip is a matrix array of 16×16 sensors and each one consists of a thin-film diode (TFD) connected in series with a MTJ (see Fig. 1) [9]. Biochip scalability is of great importance in biodetection applications as it enables analysis of a larger number of different targets in parallel. Such biochips could, for instance, be used in clinical diagnostics of genetic diseases characterized by a large number of mutations (over one hundred), like in cystic fibrosis [6].

In the developed system, the biochip is integrated in a new miniature [credit card dimension, see Fig. 1(b) and 19] hand-held platform incorporating all electronics for addressing, reading out, sensing, temperature controlling and fluid sample handling [10]. Since readout signals have very small amplitude (about 15–20 μV_{rms}/bead, for 250-nm particles), advanced signal processing techniques are implemented in a digital signal processor (DSP). The DSP processes the recovered

Manuscript received December 16, 2005; revised August 1, 2006. This work was supported in part by Fundaçao para a Ciécia e a Tecnologia (FCT) under Project POSI/EEA-ESE/58523/2004. This paper was recommended by Guest Editor P.-C. Chung.

M. Piedade, L. A. Sousa, T. M. de Almeida, J. Germano, B. A. da Costa, and J. M. Lemos are with the Electrical and Computers Engineering Department, Instituto Superior Técnico, Technical University of Lisbon, 1000-029 Lisbon, Portugal, and also with Instituto de Engenharia de Sistemas e Computadores-R&D (INESC-ID), 1000-02 Lisbon, Portugal (e-mail: msp@inesc-id.pt; las@inesc-id.pt; teresa.almeida@inesc-id.pt; jahg@inesc-id.pt; bac@inesc-id.pt; jlml@inesc-id.pt).

P. P. Freitas, H. A. Ferreira, and F. A. Cardoso are with the Physics and Computers Engineering Department, Instituto Superior Técnico, Technical University of Lisbon, 1000-029 Lisbon, Portugal, and also with the Instituto de Engenharia de Sistemas e Computadores-Microsistemas & Nanotecnologias (INESC-MN), 1000-029 Lisbon, Portugal (e-mail: pfreitas@inesc-mn.pt; hferreira@inesc-mn.pt; fcardoso@inesc-mn.pt).

Digital Object Identifier 10.1109/TCSI.2006.884420

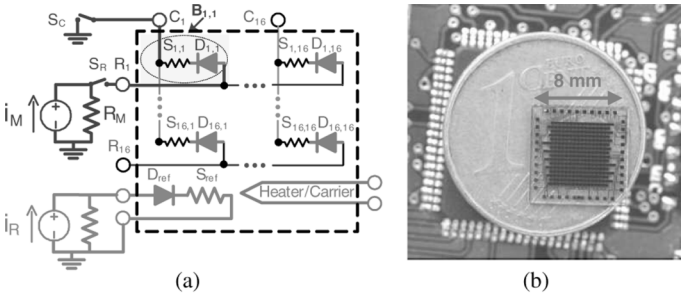

Fig. 1. Magnetoresistive biochip. (a) Simplified electrical scheme. (b) Photograph.

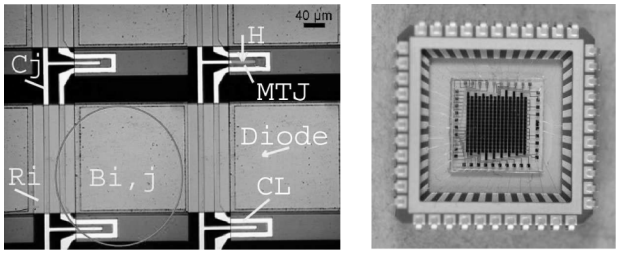

Fig. 2. Magnetoresistive biochip detailed. (a) Microphotograph of matrix cells. (b) Encapsulated biochip.

signals, reduces noise and offset effects and controls biochip temperature. The analogue circuitry, which was optimized and reduced to the minimum, is controlled by the DSP, replacing conventional bulky lock-in analogue amplifying techniques. High-level system control and data analysis are remotely performed through a personal digital assistant (PDA) via a wireless channel or a universal serial bus (USB).

This paper presents the proposed architecture for the handheld platform and discusses the details of biochip design, fabrication, modelling and reading techniques. The paper is organized as follows. Sections II and III present the biochip main characteristics. Section IV details the proposed architecture and Section V gives some description of the implemented prototype. In Section VI experimental results are presented. Finally, in Section VII, relevant conclusions are drawn and directions for further research are pointed out.

II. Biochip Technology

The system is based on a new type of magnetoresistive biochip, fabricated at Instituto de Engenharia de Sistemas e Computadores-Microsistemas & Nanotecnologias (INESC-MN), Lisbon, Portugal, using standard microfabrication techniques. As depicted in Fig. 1, each biosensor detection site incorporates a TFD, $D_{i,j}$, in series with a magnetoresistive sensor, based on an MTJ, $S_{i,j}$, leading to a matrix-based biochip. Each TFD has two main functions: 1) to act as a switching device enabling the connection between column C_j and row R_i of the matrix; 2) to act as a temperature sensor of each biosensor site, $B_{i,j}$. The MTJ is very close to the TFD [see Fig. 2(a)] and operates as a sensor of the planar magnetic field H transversal to its length. The MTJ is also slightly temperature dependent as it will be shown.

In each biosensor site $B_{i,j}$ [Fig. 2(a)], an electric current flows from row conductor R_i (large transversal metal conductor), through the TFD into the MTJ (perpendicularly to the plane of the photograph), and finally to column conductor C_j. The biochip has a configuration of 16×16 cell matrix integrating hydrogenated amorphous silicon (a-Si:H) TFDs with aluminum oxide barrier MTJs [6].

Each detection site also incorporates a patent-pending U-shaped carrier line (U-CL) structure [Fig. 2(a)] that has two main purposes: 1) to generate a magnetic field to sweep target biomolecules at low frequencies over the immobilized probes increasing the hybridization rate; 2) to heat biochip sites. The CL [carrier-heater, see also Fig. 1(a)] has approximately 60 Ω of total resistance and is divided in four lines associated in series, each one with 15 Ω, surrounding 64 biochip sensors. By using the U-CLs it is possible to implement different objectives and strategies for temperature control of the biochip four subregions.

Layers of different materials are deposited over a glass substrate by an ion beam deposition or by magnetron sputtering and are defined by direct write laser lithography and ion milling. The TFDs are Schottky-barrier diodes formed at the interface of an a-Si:H thin film and an aluminum lead and their size is 200 μm $\times$ 200 μm. MTJ sensors are 10 μm $\times$ 2 μm in size and comprise an anti ferromagnetic layer (MnIr thickness of 250 Å), a fixed ferromagnetic layer (50 Å of CoFeB), a tunnelling insulating barrier (12 Å of aluminum oxide) and a free layer (15 Å of CoFeB+45 Å of NiFe). These transducers show a relative change in resistance (tunnelling magnetoresistance ratio—TMR) of 27%. In addition, a microfluidic chamber with volume of 5 mm $\times$ 5 mm $\times$ 0.5 mm is mounted over the encapsulated chip [Fig. 2(b)]. A plexiglass window is provided with two fluid ports, where two silicone tubes (2 mm of external diameter) can be connected to the fluid dispenser.

When the biosensor is used for detection of DNA hybridization, the site over each MTJ transducer is previously functionalized with a DNA probe, as represented in Fig. 3(a). The target DNA, tagged with paramagnetic nanoparticles, is transported in fluid and focused at sensing sites using alternating magnetic field gradients created by the U-CLs. Subsequently, the DNA target hybridizes with the available complementary probe and finally, the magnetic labels remain bound to the surface of the sensors after washing the chip with a buffer solution (see Fig. 3).

The application of a dc or an ac external magnetic field induces a magnetic moment on the nanospheres and each MTJ sensor detects this change depending on the number of labels bound to its surface. In the system described in this paper, the reading magnetic field (H, in Fig. 3) is generated by an external coil or, alternatively, by appropriate electric currents circulating in the carrier lines.

III. Biochip Characterization and Modelling

Each matrix element is driven with a measuring current, i_M, and small changes of the MTJ resistance are read as small voltage changes at the input driving port. Each biosensor element (TFD+MTJ) may then be characterized by a large-signal model (Fig. 4) which takes into account the biosensor measured voltage, v_M, nonlinear relationship with the measuring current,

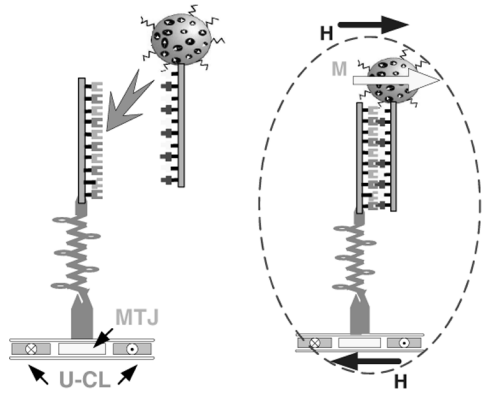

Fig. 3. DNA hybridization. (a) Magnetically labelled DNA targets are focused at DNA probe functionalized sites by use of on-chip carrier line structures. (b) DNA hybridization is detected through the sensing of the magnetic stray fields created by the labels using a MTJ transducer.

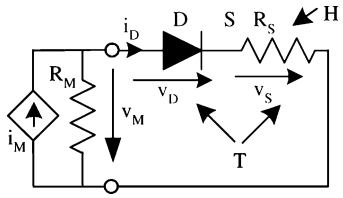

Fig. 4. Biosensor element large-signal model.

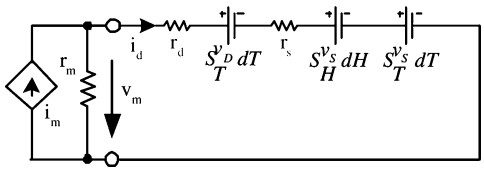

Fig. 5. Biosensor element small-signal model.

i_M, absolute temperature, T, and external magnetic field, H, through the TFD and MTJ voltages (v_D and v_S, respectively)

$$v_M = v_D(i_M, T) + v_S(i_M, T, H). \tag{1}$$

A small-signal model (Fig. 5), valid near a quiescent point (I_M, T, H), may be derived

$$dv_M = \underbrace{\frac{\partial v_D}{\partial i_M}}_{r_d} di_M + \underbrace{\frac{\partial v_D}{\partial T}}_{S_T^{v_D}} dT + \underbrace{\frac{\partial v_S}{\partial i_M}}_{r_s} di_M + \underbrace{\frac{\partial v_S}{\partial H}}_{S_H^{v_S}} dH + \underbrace{\frac{\partial v_S}{\partial T}}_{S_T^{v_S}} dT. \tag{2}$$

This proposed small-signal model does not take into account noise components that may be generated in the TFD or in the MTJ (shot noise, thermal noise and $1/f$ noise), because biosensor noise contribution will be filtered out.

A. TFD Electrical Characterization and Modelling

The *I–V* characteristic of an amorphous TFD is slightly different from the *I–V* characteristic of a crystalline semiconductor junction due to the space charge limited current (SCLC) phenomena [11], that typically occurs in amorphous semiconductor films. In order to achieve a very good *V–I* characterization regardless current range, a compound model, including the semiconductor junction voltage drop v_J and a compound bulk voltage $v_A + v_B$ that varies nonlinearly with current, is considered for the TFD

$$v_D = \underbrace{n \times V_T \ln\left(\frac{i_D}{I_s} + 1\right)}_{v_J} + \underbrace{(i_D R_A)^{\alpha}}_{v_A} + \underbrace{(i_D R_B)^{\beta}}_{v_B} \tag{3}$$

where n is the emission coefficient, $V_T = KT/q$ is the thermal voltage, and I_S is the diode saturation current. The first two terms of the sum v_J and v_A, lead to a very good characterization of the TFD for low and medium current/voltage values. When a global model is desired in order to include the high current/voltage region, the second nonlinear term v_B must be added. The proposed compound model allows a better characterization of TFD behaviour in the high current/voltage region (an operating upper limit of $\approx 70\ \mu$A is assumed for reasons explained below). The two last contributions, v_A and v_B, may be seen as the contributions of two nonlinear resistors.

Fig. 6 depicts the *I–V* experimental characterization (circle marks) of one of the 256 TFDs of the biochip, at room temperature of 24 °C and at 40.5 °C. It can be seen that, at room temperature [Fig. 6(a)], TFDs are very well modelled by *model A* (two first terms) in the low/midle region but only *model B* (complete model) may achieve a good match with experimental data in the high current/voltage region. Only for extremely high currents/voltages the proposed model differs slightly from experimental data. For higher temperature values only the compound model achieves a good characterization (see Fig. 6(b) for 40.5 °C).

For the proposed model, the TFD incremental resistance is

$$r_d = \frac{nV_T}{i_D + I_S} + \alpha R_A^{\alpha} i_D^{\alpha-1} + \beta R_B^{\beta} i_D^{\beta-1}. \tag{4}$$

Fig. 6(c) shows the TFD r_d (same conditions as before), both calculated directly from experimental data (circle marks) and through the considered models (dashed and solid lines). As in the *I–V* characteristic, it can be seen that *model B* may achieve a better characterization. Only for extremely high currents, where the biosensor will not operate, due to MTJ current limitations, the proposed model differs from experimental data.

B. TFD Temperature Characterization and Modelling

The temperature of each biochip matrix element carries relevant information to characterise and analyze the DNA hybridization that occurs in the site placed over the magnetic biosensor. The TFD *V–T* characteristic is used for measuring this temperature because the TFD is implanted very close to the magnetic sensor [see Fig. 2(a)] and has a very good thermal connection with it. If the TFD is fed with a very small constant current I_D, voltage drop V_J dominates over V_A and V_B, and V_D varies almost linearly with temperature T, although it depends on technological junction parameters (c_S, ω, n, and E_G) [11] due to I_S

$$I_S = c_S T^{\frac{\omega}{n}} e^{-\frac{E_G}{nV_T}}. \tag{5}$$

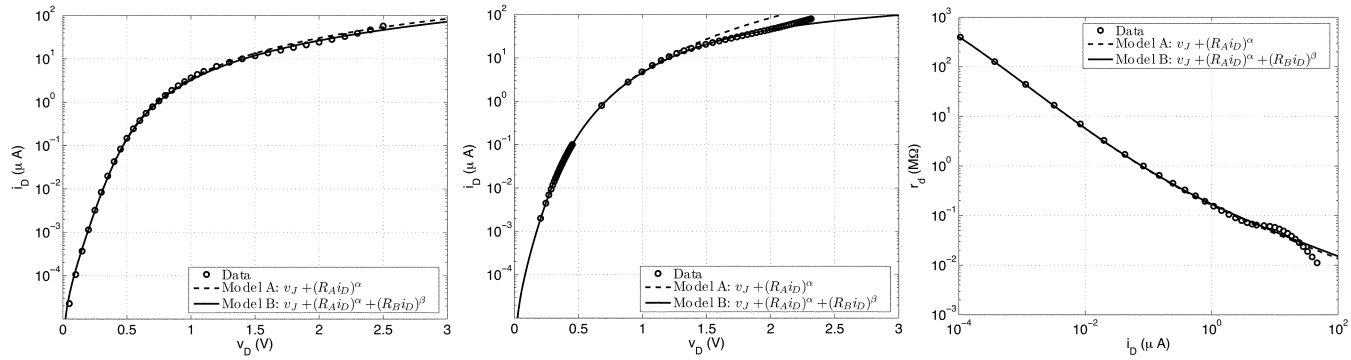

Fig. 6. TFD *I–V* characteristic and incremental resistance. (a) *I–V* at 24 °C. (b) *I–V* at 40.5 °C. (c) r_d at 24 °C.

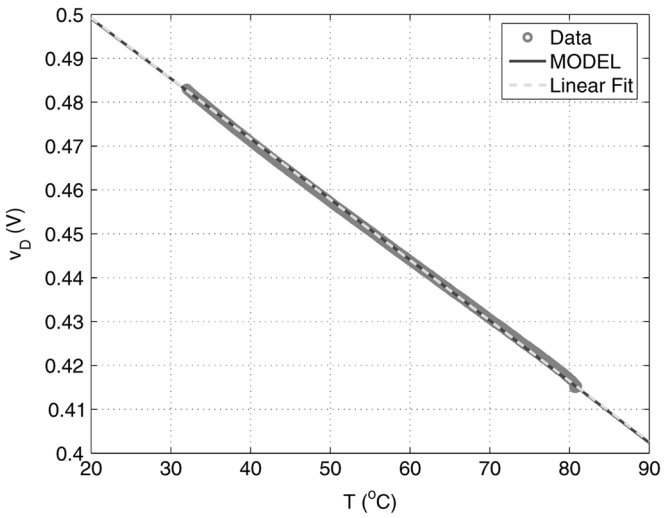

Fig. 7. TFD *V–T* characteristic for $I_D = 100$ nA.

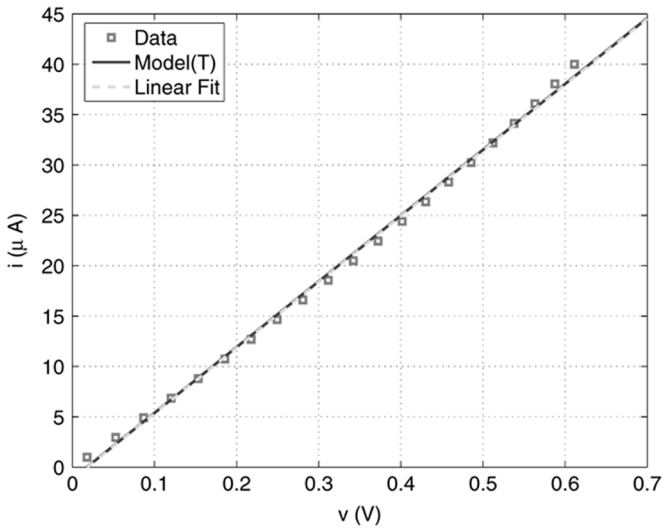

Fig. 8. MTJ *I–V* characteristic at 30.4°C.

The sensitivity of the *V–T* characteristic, for low i_D values, may then be calculated at a quiescent point (I_D, V_D, T) as

$$S_T^{v_D} = S_T^{v_J} + S_T^{v_A+v_B} = \frac{V_D - \omega V_T - E_G}{T} + \frac{\partial (v_A + v_B)}{\partial T}. \tag{6}$$

For low current values $S_T^{v_A+v_B} \ll S_T^{v_J}$ and the second term may be neglected, leading to $S_T^{v_D} \approx S_T^{v_J}$, which corresponds to an almost linear characteristic (for a certain temperature range). This linear behaviour is exhibited by experimental data shown in Fig. 7 (circle marks) when the TFD was fed with a small constant current of 100 nA. A direct linear fit over data leads to $S_T^{v_D} = -1.38$ mV/°C (dashed line), while, on the other hand, estimating technological parameters from data ($n = 1.0286, c_S = 1.22453 \times 10^{-5}, w = 1.63233, E_G = 0.85824$) leads to $S_T^{v_D} = -1.37$ mV/°C (solid line).

Because the TFD temperature characteristic depends on technological parameters, each sensor needs to be calibrated in a certain temperature range. For a given, small and constant current, voltage $v_D(T)$, at a temperature T, can be estimated using a known value $v_D(T_0)$ at a reference temperature T_0, through linear interpolation. Higher order interpolating schemes may be considered whenever higher current values cause sensitivity to deviate from a linear characteristic.

C. MTJ Electrical and Temperature Characterization and Modelling

Each MTJ has an *I–V* characteristic that is almost linear, as can be observed in Fig. 8 (square marks represent experimental data). A linear model with constant coefficients may then be considered, $i = i_0 + R_0^{-1} v$, and $R_0 = 15.32$ kΩ and $i_0 = -1.197$ μA were obtained for 30.4 °C (solid line). Due to the ultra thickness of the dielectric needed to obtain tunnelling effect, typical MTJs may breakdown for applied voltages over 1.1 V. This fact limits the maximum secure driving current to ≈70 μA for a MTJ with a nominal value of R_0.

Although R_0 is slightly temperature dependent in a linear way, due to its low sensitivity and the fact that each MTJ is always in series with a TFD, it is possible to consider that it is almost temperature independent. Experimental results (square marks in Fig. 9) evidence R_0 temperature dependence. Assuming a linear model and considering the estimated values

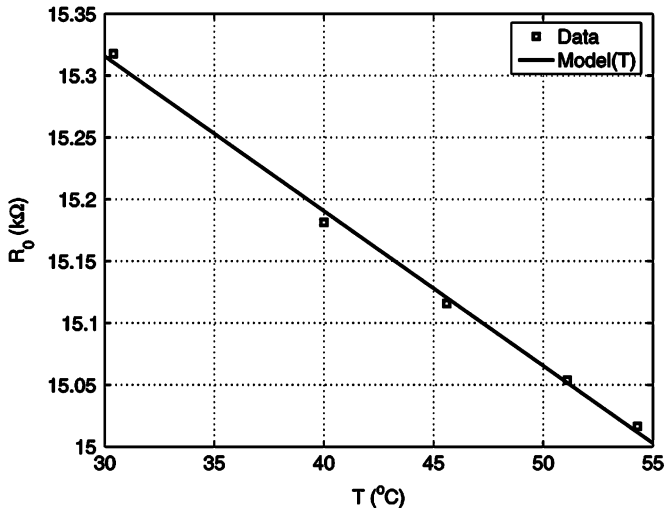

Fig. 9. MTJ R_0 temperature dependence.

$R_0(T)$, it is possible to obtain $dR_0/dT = -12.52\ \Omega/°\text{C}$ and $R_0(0) = 15.69\ \text{k}\Omega$.

Assuming this temperature dependent model and considering all estimated parameters, Fig. 8 also depicts the expected voltage drop for each drive current value. For a drive current of 1 μA a sensitivity of $-12.52\ \Omega/°\text{C}$ corresponds to a voltage drop sensitivity of $S_T^{v_S} = -12.52\ \mu\text{V}/°\text{C}$ which is negligible when compared with $S_T^{v_D} = -1.37$ mV/°C exhibited by the TFD that is in series with the MTJ. From what was stated before and these experimental results and models, it can be inferred that it is possible to use each TFD as a site temperature sensor and neglect the MTJ very low temperature sensitivity.

D. MTJ Magnetic Characterization

The MTJ resistance also changes with the transversal component of an applied magnetic field H. Its sensitivity to the magnetic field is measured through the tunnelling magnetoresistance ratio (TMR). A maximum change occurs when no voltage is applied to the tunnel junction

$$\text{TMR}(0) = (R_{\max} - R_{\min})/R_{\min} \times 100\% \tag{7}$$

where $R_{\max}$ and $R_{\min}$ are the maximum and minimum resistance values obtained with magnetic opposite saturation fields (typically ± 10 Oe, $\Delta H_{\max}$). The TMR signal is almost constant until 30 mV (an initial value of $\text{TMR}(0) \cong 27\%$ was obtained for the technology used in the biochip) and then starts to decrease almost linearly with bias voltage increase. The decreasing rate is almost constant in the range where the signal drops to half the initial value at 300–500 mV ($V_{1/2}$ in Fig. 10). In the range 300–500 mV it is possible to model

$$\text{TMR}(V) = \text{TMR}(0)\left[1 - \frac{V}{2V_{1/2}}\right] \tag{8}$$

showing that the MTJ TMR increases with the decrease of the dc bias voltage applied to it.

However, if resistance is constant the reading signal, v_M, increases with current. This means that there is a tradeoff between these two phenomena and a maximum voltage variation, $\Delta V_{\max}$, is observed at a certain current. This current value depends on the MTJ resistance: the higher the resistance, the lower

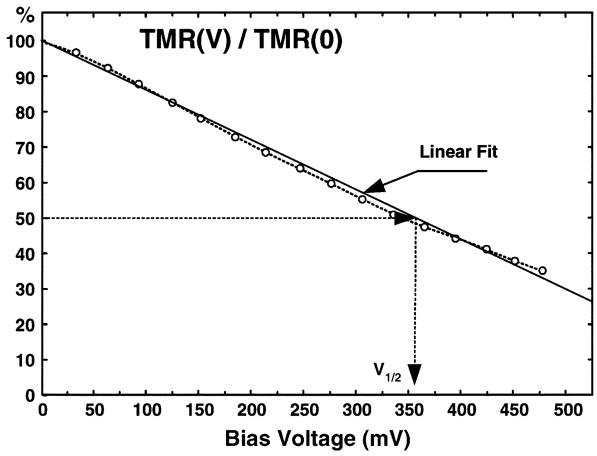

Fig. 10. TMR dependence with bias voltage.

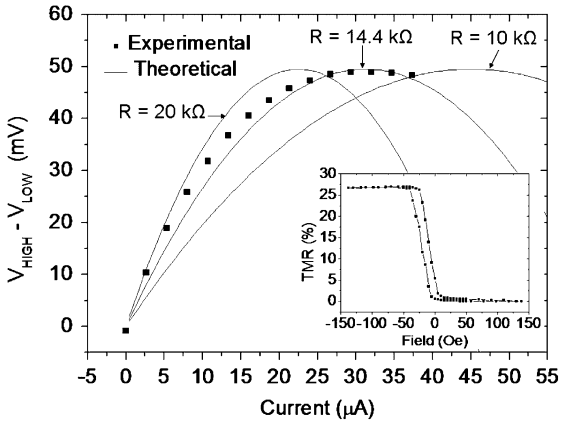

Fig. 11. MTJ voltage variation dependence with drive current.

will be the current value at which the maximum is observed (Fig. 11). Its value may be derived through

$$S_H^{v_S} = \frac{\partial v_S}{\partial H} = S_H^{R_S} \times i_M = \text{TMR}(V)\frac{R_S}{\Delta H_{\max}} \times i_M \tag{9}$$

and may be estimated as $V_{1/2}/R_S$.

Experimental characterization of one of the biochip MTJs showed a resistance of 14.4 kΩ and the voltage variation maximum occurs for a drive current of $\approx$30 μA (see Fig. 11). Device simulations for three different MTJ resistances (10, 14.4, and 20 kΩ) are also shown and agree well with experimental data. The decrease of ΔV for higher bias currents is caused by TMR decrease at increasing bias voltage. For biochip applications a maximum voltage variation is desirable.

Increasing MTJ resistance decreases current values required to maximize signal output but at the expense of increased sensor noise (mostly $1/f$ for low-frequency applications). For the present TFDs, currents in excess of a few hundred μA will cause irreversible damage. MTJ area and $R \times A$ values must be optimized for maximum tolerable current through the TFD.

E. Reading the Biosensor

The reading of each biochip cell is performed several times and the obtained results are low-pass filtered and averaged by

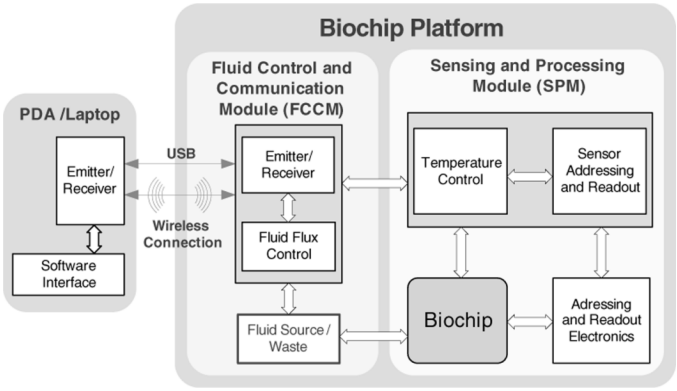

Fig. 12. Block diagram of the biochip platform architecture.

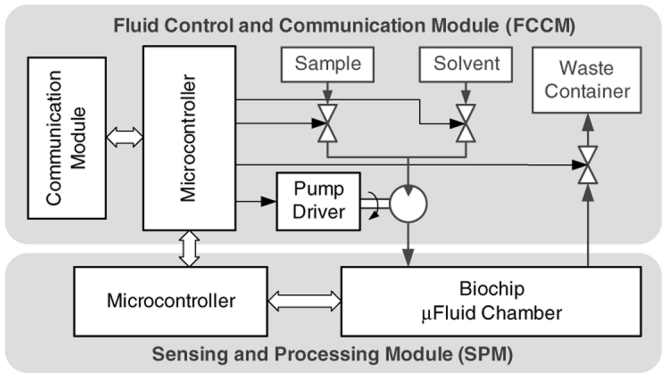

Fig. 13. Block diagram of the fluid flux controller.

the DSP. The proposed biochip platform has an excellent flexibility leading to a lot of alternate reading techniques.

Stated in a simplified way, one of the various available reading procedures may be envisaged through a set of ten steps: 1) to choose the common mode of amplification for the instrumentation amplifier and set it with a minimum voltage gain; and 2) for each addressed site, drive the chip with a set of very small currents and measure the corresponding dc voltages; calculate TFD parameters and in site temperature using the exponential portion of its *I–V* characteristic; swept current in order to generate and store each TFD *I–V* characteristic; choose a differential configuration for the instrumentation amplifier; set up an appropriate current drive for the sensor and output the corresponding voltage stored in *I–V* characteristic; drive the external coil that generates transversal magnetic field with an ac current; set the amplifier gain ensuring no output voltage saturation occurs; digitally filter the acquired signals with a small bandwidth bandpass filter; measure the acquired rms value of the signal originated in the biosensor, which is related to the number of magnetic beads placed over the sensor.

Two methods are considered in order to control the biochip temperature: overall heating using the U-CLs; and heating using a persistent reading of each cell with higher current values. In this procedure, a temperature reading cycle (small currents) alternates with a heating cycle (larger currents) in order to increase site temperature.

IV. Platform Architecture

As depicted in Fig. 12, the proposed modular architecture for the biochip platform is organized into two main modules: 1) the sensing and processing module (SPM); and 2) the fluid control and communication module (FCCM). The SPM integrates the biochip and provides the circuits that directly interact with the array of biosensors (biochip), in order to individually address the sensors and readout data from them, and to control the temperature in the different sub-areas of the biochip. The FCCM interfaces the platform with the external world, by controlling the fluid carrying the magnetically tagged biomolecules and providing wireless communication with a hand-held analyzer, based on a PDA. The graphical user interface (GUI) and information processing and classification algorithms are hosted within the hand-held device, taking advantage of its computing power and input/output peripherals. In fact, the biochip platform is a peripheral itself of the PDA, which can be a pocket PC or a laptop.

The biochip is integrated in the central module of the platform, which generates the electrical signals to drive the sensor array and to individually address and readout signals provided by each sensor. Moreover, it is also in charge of individually measuring and controlling temperature in subsections of the biochip, by using the CLs or by taking advantage of the TFD *V–T* characteristic derived in Section III.

Sensor addressing is based on a commutating matrix of integrated TFDs, each one acting as a switch in series with the corresponding MTJ magnetoresistive sensor. The microcontroller provides the row/column addresses of the sensor to read and define the drive current through a digital-to-analog-converter (DAC). This allows the usage of a single DAC and a single instrumentation amplifier to drive and to read all the sensors in the array. These are the only analog circuits, since control and signal processing are performed by digital processors associated to 1-Mbit memory for storing the processed data to be transmitted to the hand-held analyzer.

The temperature sensors are calibrated by programming the digital processor to generate current pulses modulated in width (PWM). The calibration is performed in dc, by amplifying the voltage at the terminals of the serial circuit in each sensing site. This calibration phase is performed at setup time in order to experimentally extract the junction parameters that allows to relate voltage with temperature. Calibration tables are filled for each sensor with absolute and differential voltages measured using reference sensors available on the chip. To measure the resistance variation of the magnetoresistive sensors, an ac excitation is performed, using an external magnetic field generated by a coil placed below the biochip. The generation of this magnetic field is digitally controlled. This ac analysis allows the measurement of small relative variances on the resistance (less than 5%) by using the differential mode of amplification; the reference signal can be generated by a microcontroller or registered from the sensors themselves in specific operating conditions.

The biochip is automatically fed with the biological material by the fluid source/dispenser controller, which generates control signals to open/close external microvalves to push the fluids in and out of the biochip. Two main operations are supported by the digital fluid flux controller (a simplified diagram is in Fig. 13): 1) to carry the fluid with the sample and the magnetic labels to the microchamber placed over the chip; and 2) to push

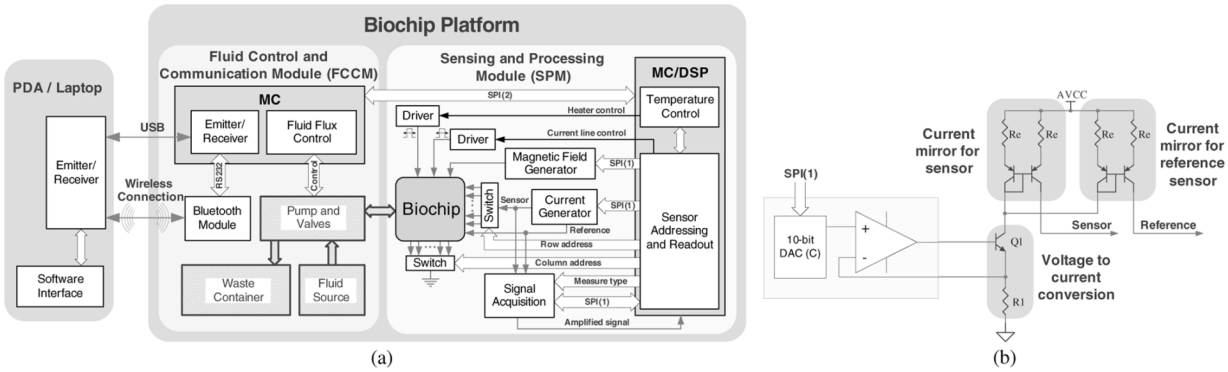

Fig. 14. Biochip platform details. (a) Biochip platform diagram. (b) Current generator circuits.

a washing fluid over the surface of the chip, in order to wash off uninteresting biomolecules and unspecifically bound markers. The order to start the operations is always received from the hand-held analyzer.

The other block of the FCCM is an emitter/receiver used to communicate through a serial bus channel, wired (USB) or wireless (bluetooth), with the hand-held analyzer.

The hand-held device acts as the master of the system, allowing the execution of a set of pre-programmed tasks. It also provides a GUI and implements the algorithms for data analysis. The PDA also acts as a logger, storing the read values for future analysis and to build a data repository. This can be useful, for example, to compare the evolution of a given parameter in a series of time-spaced tests.

V. Prototype

This section is focused on the prototype implementation of the different modules, both hardware and software components. The presented implementation corresponds to a small autonomous platform, hand-held, capable of performing sample analysis. Fig. 14(a) depicts the two main modules of the architecture that correspond to two printed circuit boards and the PDA for user interface and high-level processing.

A. Main Board

The core of the system is a 16-bit integrated microcontroller (MC/DSP), the Microchip dsPIC 30F6014. It has a performance of up to 30 million instructions per second (MIPS) and an extended instruction set for digital signal processing [12]. It communicates with the microcontroller in the auxiliary board trough the serial peripheral interface (SPI). It is programmed to perform a set of pre-defined tasks, according to the commands received from the PDA. This MC/DSP addresses and reads data from the array of magnetoresistive sensors provided by the biochip and measures and controls temperature through the same devices. To perform all these operations, the MC/DSP controls the circuits represented in Fig. 14(a) and described in the next subsections.

1) Current Generators: The biochip matrix is driven by a dc current or by a dc current with a small superimposed ac component. The current is generated using a DAC and a voltage-to-current converter [Fig. 14(b) depicts a simplified diagram of the circuit]. Current is generated through $R_1, I_{\mathrm{Sens}} = I_{\mathrm{Ref}} = V_{\mathrm{DAC}}/(2R_1)$, where V_{DAC} is the DAC output voltage. A reduced number of reference sensors are placed in different subareas of the biochip for reference purposes.

The current for the external coil is generated by a similar circuit to the one depicted in Fig. 14(b), but the current mirror is replaced by a coil and a free wheel diode.

2) Addressing Circuits: To address and read the sensor array, the sensor current is demultiplexed/multiplexed using two sixteen channel switches with very low resistance in the ON state and high channel matching. The voltage across each matrix element (TFD plus magnetic sensor) is measured.

The biochip also includes a carrier circuit, represented in Fig. 2, which generates local magnetic fields through the CLs to guide the target biomolecules over immobilized biological probes. The current required for this circuit is generated using the MC/DSP PWM output ports. The only required external component is a MOS transistor operating as a switch. The heater circuit (represented in Fig. 1) provides thermal power that can be controlled in order to ensure the required temperature changes. This circuit is also implemented using a PWM port output and a transistor.

3) Signal Acquisition: Electronic circuits for signal acquisition are represented in Fig. 15. The signals connected to the amplifier stage are defined using two switches. Hence, this circuit can provide several measurement types, ac or dc, and use different references: 1) measuring by using a reference sensor (differential); 2) measuring without reference sensor (non differential, the reference is the circuit ground); and 3) measuring by using a calibration value as reference (differential). The architecture (see Fig. 15) allows the extraction of a differential voltage between each matrix element and reference elements placed in the biochip. To overcome mismatches between sensors, each sensor uses oneself as a reference. At the calibration phase, matrix elements are scanned with scaled currents and calibration tables are built. These registered values are used as references at the next reading phase.

On the amplification block, the dc gain has a range between 1 and 20 and the ac gain can be set from 50 to 1000. The amplified signal is then converted to the digital domain using a high resolution sigma-delta converter or a successive approximation faster analog-to-digital converter (ADC). These faster converters are used to read the sensor temperature even during the acquisition phase when the sensor signal is converted by the high-resolution low-speed ADC.

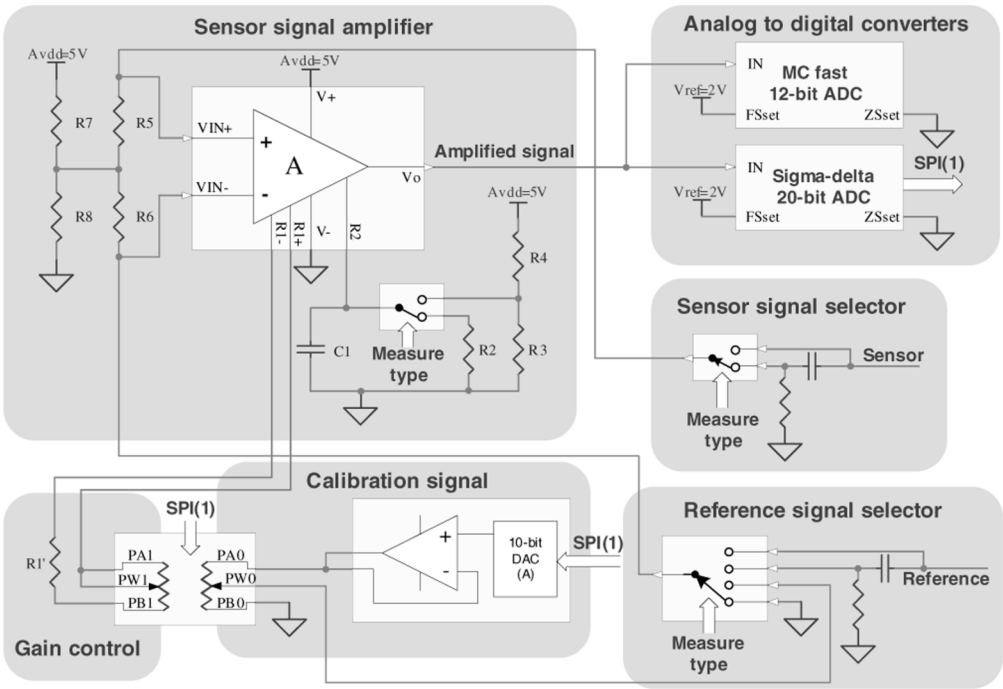

Fig. 15. Circuit diagram of the sensor reading.

4) SPM Configuration and Programming: The MC/DSP perform several tasks beyond reading the biochip. The biochip reading involves the following phases: calibration, temperature control and signal measuring. Furthermore, there are several types of measurements that can be selected. The PDA acts as master for the entire system and determines which type of measure should be performed and, in the end, it receives the collected data after a pre-processing at the MC/DSP. The system is in sleep mode until a user action takes place and a measurement type is selected and send from the PDA to the biochip platform. After that, the system enters a cycle of calibration, sensor measurement and transmission to the PDA until all 256 sensors are read.

At the calibration phase, the ambient temperature is known and no magnetic field is applied to the sensor. Each matrix element is driven with sequentially increased scaled constant current values, N sensor values are acquired for single sensor current and these values are processed to decrease the noise. These values are stored in MC/DSP memory and are used in future biochip readings.

For temperature control, a cycle is associated with a timer interruption which becomes active when a sensor reading takes place. Using the read sensor value, the current temperature can be calculated and used to determine the new duty cycle for the PWM current line controller.

At the measuring phase, the MTJ resistance variation due to the magnetic particles captured over each sensor must be measured. A burst of an ac current, superimposed to a dc biasing current, is generated by the MC/DSP, and it is applied through the addressing circuits to each matrix element. The measure can also be performed using only a dc bias current and an ac magnetic field (internal or external to the biochip). The sensor signal is digitized and is processed by the MC/DSP through digital signal processing algorithms.

B. Communication System and Fluid Control

As stated before, to allow a flexible and easy operation, the biochip platform is controlled from a PDA. Two types of communication can be used to control the platform: a wireless connection using the bluetooth protocol or a USB connection.

The bluetooth uses a fully integrated class 2 module [13]. This module has a maximum output power of 2.5 mW and a typical range of 20 m. The firmware supplied with this device offers a complete bluetooth (v1.1) stack including profiles and command interface. It also provides the generic access profile (GAP), the service discovery application profile (SDAP), and the serial port profile (SPP). This firmware features point-to-point and point-to-multipoint link management, supporting data rates up to the theoretical maximum of 704 kbps. This module is linked to the peripheral control module via an UART interface.

For the USB, a microcontroller from Microchip that includes a USB interface was adopted [14]. This device features an USB communication module that is compliant with the USB specification revision 2.0. The module supports both low-speed and full-speed communication for all supported data transfer types. The programming in the master device is performed using a dynamic link library (DLL) module that provides wrapper functions for the Microchip general purpose USB Windows driver.

The transmitted messages are processed at the FCCM and then packed and send over a SPI connection to the SPM. There are two exclusive messages that are used to terminate or to initiate the biochip operation. Before any measurement takes place it is necessary to deploy the fluid over the sensors. When all the readings are done with a given sample, the biochip must be washed. Both these operations are controlled by the FCCM. If any other command is received the data is transmitted to the SPM. The data transfer between the processing platform and the communication platform is done using an SPI interface.

C. PDA User Interface

The interface with the biochip platform was tested using a PDA from Fujitsu Siemens, a Pocket Loox 720 with an Intel XScale PXA 272, 520-MHz processor, 128-MB RAM memory, Bluetooth 1.2 and USB 1.1 host capabilities. The graphical interface software to the PDA has been developed using Microsoft embedded Visual C++ 4.0 environment [15]. The system was designed to perform several types of measurements and also to act as a data logger, providing the capability to compare results from different experiments. The developed GUI provides a simple and user friendly interface, being suitable for users less familiar with computer devices.

VI. Experimental Results and Limitations of the Proposed System

Several experimental results have been presented all through the paper, especially in Section III, where the proposed models were confronted with experimental data characterization of the biochip elements. TFD *I–V* and incremental resistance characteristics were measured for different temperatures (Fig. 6), allowing the proposed models parameters estimation. The TFD *V–T* characteristic for a constant current was also characterized and TFD technological parameters considered in the proposed model were estimated (Fig. 7). The agreement between experimental data and the proposed model showed a linear characteristic indicating that the TFD may be used as a temperature sensor with a sensitivity of -1.37 mV/°C. MTJ electrical, temperature and magnetic characterization was also performed. Biochip MTJs showed resistance values typically of 15 kΩ and a sensitivity of -12.52 Ω/°C (Fig. 9), which, for a current of 1 μA, leads to a voltage sensitivity of -12.52 μV/°C that is negligible when compared with -1.37 mV/°C exhibited by the TFD that is in series with it. These results prove that the TFD may be used as a temperature sensor. MTJ magnetic characterization showed that there is an optimum current value ($\sim$30 μA) leading to a maximum voltage variation of 50 mV (Fig. 11).

The biochip small-signal frequency response was analyzed and it was determined that, due to the MTJ extremely small size, its associated capacitances are very small and, as a consequence, its cutoff frequency is very high (beyond the reading platform limit). However, due to the big size of the TFD its capacitances (diffusion capacitance for forward bias and junction capacitance for reverse bias), associated with the large resistor due to the SCLC phenomenon, already referred, lead to a low-pass frequency response for the biosensor with a low cutoff frequency. The biosensor reading was then performed by measuring the input voltage v_M (Fig. 4) obtained by feeding a small ac current superimposed over the dc bias. The reading speed of each biosensor depends mainly on the time and frequency responses of the associated TFD.

Fig. 16 shows the amplitude of the frequency responses of v_m (Fig. 4), when an ideal current source, shunted with a 100 kΩ resistor, was used to directly drive the TFD (the MTJ was short-circuited). Three different bias current values were considered (150 nA, 3.5 μA and 10 μA) to which a very small ac current signal was added. For a 150 nA of bias current (0.5 V of V_D bias) a -3-dB cutoff frequency of 11.8 kHz and a dc gain of -0.9 dB were obtained (line 1). When the diode was biased

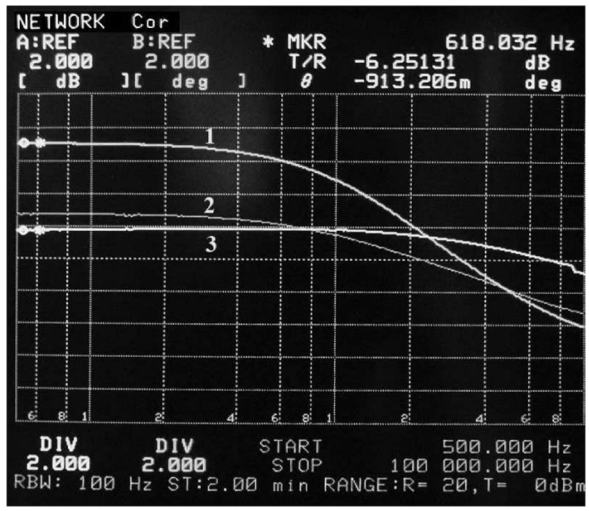

Fig. 16. TFD amplitude frequency response for three typical bias current values: (1) 150 nA. (2) 3.5 μA. (3) 10 μA.

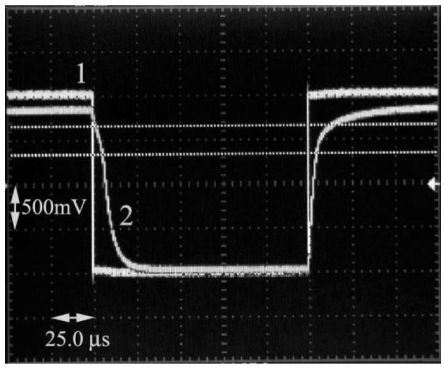

Fig. 17. TFD time response. (1) Input signal. (2) Output signal.

with 3.5 μA ($V_D = 1$ V), a cutoff frequency of 24 kHz and a dc gain of -5.26 dB were obtained (line 2). Finally, a bias current of 10 μA ($V_D = 1.5$ V) led to a -6.25 dB dc gain and a cutoff frequency of 200 kHz (line 3). These results show that the TFD impedance decreases with frequency as expected and, as a consequence, v_m decreases with frequency, exhibiting a low-pass frequency response. In conclusion, the biosensor frequency response is expected to have a minimum cutoff frequency of at least 10 kHz, which will impose an upper limit on the biochip platform reading frequency.

The TFD high-level commutating behaviour was also studied and the time response for one of the chip biosensor TFDs is shown in Fig. 17. It was measured with a 10 MΩ//10 pF probe and the TFD was driven with a 4 kHz square wave with 1 V of amplitude and a source resistance of 100 kΩ (this voltage source corresponds to a 10 μA current source shunted with a 100 kΩ resistor, see Fig. 5). Experimental results show that the TFD turn off time is 10 μs and the turn on time is about 50 μs. Considering an additional ac reading time, a maximum safe commutation rate of about 5 kHz is obtained which leads to an expected total biochip reading rate of about 20 Hz.

The noise generated by a typical biosensor presented in this paper was measured. For an operating frequency of 400 Hz, the TFD contributes with a voltage noise of 98 nV/$\sqrt{\text{Hz}}$ and 79 nV/$\sqrt{\text{Hz}}$ for the currents $I_D = 7.3$ μA and $I_D = 67.3$ μA,

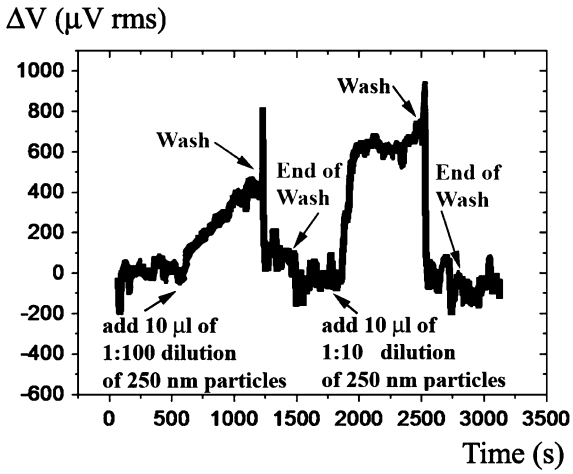

Fig. 18. Output of the MTJ detecting the effect of an external transversal magnetic field of ± 10 Oe over nanomagnetic spheres in a fluid with different concentrations.

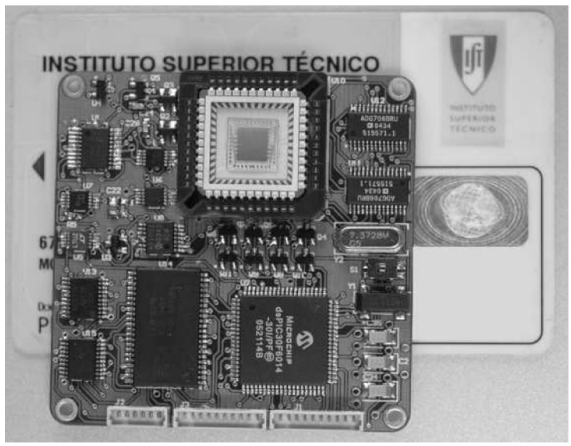

Fig. 19. Picture of the prototype main board.

respectively. This is essentially 1/f noise. The MTJ with $R = 27$ kΩ contributes with a total noise, including the magnetic one, of 290 nV/$\sqrt{Hz}$, mainly thermal noise because 1/f corner frequency is about 450 Hz. Therefore, the total noise for the biosensor is about 306 nV/$\sqrt{Hz}$. Even for a large measuring bandwidth of 50 Hz, the noise is only about 2.16 μV, lower than the resolution of the proposed system, which in the current version is about 8 μV.

The biological response of the biochip to 250-nm diameter magnetic nanoparticle solutions at two different dilutions is shown in Fig. 18. Upon particle settling over the sensor, detection signals of 450 μVrms and 650 μVrms were obtained for 10 μl of 1:100 and 1:10 (10^{11}particles/ml) dilutions, respectively.

Regarding the developed prototype, Fig. 19 presents a real size picture of the microsystem. The overall functionality of the implemented prototype has been thoroughly tested and experimental results have been collected. The microcontroller 18F4550 and the microcontroller with the instruction set extension for digital signal processing, the dsPIC 30F6014, were both mainly programmed in the C language. After profiling, segments of the code are now being tuned by using assembly language.

Power consumption of the developed prototype is relatively high for the purpose of having an autonomous platform. Operating at a voltage of 5 V, the maximum power consumption of the board is 750 mW. This maximum value occurs when the dsPIC operates at its maximum internal frequency of about 120 MHz. The power consumption drops to around 300 mW whenever the dsPIC operating frequency is reduced to one quarter of its maximum value.

To achieve maximum resolution it is necessary to reduce noise by reading each sensing element several times. Experimental results show that the time to scan all the sensor array and to process the corresponding data has an order of magnitude of 1 s, but it can be increased up to 4 s if more reads were performed for each sensor.

The present biochip is limited to 256 probe sites for a chip with 64 mm^2, a density much larger than that obtained with traditional microarrays read by laser. The density is actually limited by diode size, but a new type of smaller diodes are now being developed for the design of the next generation of the proposed biochip. The biochip platform sensitivity is now limited by the noise generated in the DAC to signals greater than 30 μV. This value may be reduced to about 8 μV by digital filtering but even this value is greater than biosensor noise. For this reason, the electronic read-out system is now being improved in order to overcome this limitation.

VII. Conclusion

This paper discusses a new hand-held microsystem architecture for biological analysis. The microsystem is based on a microchip with a matrix array of 16×16 sensors, each consisting on a thin-film a-Si:H diode connected in series with an aluminium-oxide barrier MTJ. Each of this detection sites incorporates a new technique based on a U-shaped current line to carry the target biomolecules over immobilized probes and to heat the biochip sites.

The biochip was experimentally characterized and modelled. Biosensor experimental results show that the proposed models may be used to predict some of its main characteristics, namely electrical and thermal behaviour. It has been shown that TFDs may be used as a linear temperature sensor and MTJs present a maximum voltage variation for an optimized bias current value. Moreover this paper shows that a device comprising a MTJ in series with a TFD can be used for nanoparticle detection. It was shown that it can be used to detect 250-nm diameter magnetic nanoparticles at two different dilutions.

A hand-held microsystem was designed based on digital microcontrollers and DSPs. The analog circuitry required for temperature control and sensors reading was reduced to a minimum and all the required processing and control are performed in the digital domain. A hand-held device acts both as the system master controller and the core for data analysis. The implemented prototype of the microsystem showed that with the proposed architecture and actual technology it is possible to implement portable microsystems for biological analysis.

REFERENCES

[1] D. L. Graham, H. A. Ferreira, P. P. Freitas, and J. M. S. Cabral, "High sensitivity detection of molecular recognition using magnetically labelled biomolecules and magnetoresistive sensors," *Biosens. Bioelectron.*, vol. 18, pp. 483–488, 2003.

[2] H. A. Ferreira, D. L. Graham, P. P. Freitas, and J. M. S. Cabral, "Biodetection using magnetically labelled biomolecules and arrays of spin valve sensors," *J. Appl. Phys.*, vol. 93, pp. 7281–7286, 2003.

[3] J. C. Rife, M. M. Miller, P. E. Sheehan, C. R. Tamanha, M. Tondra, and L. J. Whitman, "Design and performance of gmr sensors for the detection of magnetic microbeads in biosensors," *Sens. Actuat. A*, vol. 107, pp. 209–218, 2003.

[4] J. Schotter, P. B. Kamp, A. Becker, A. Pühler, G. Reiss, and H. Brückl, "Comparison of a prototype magnetoresistive biosensor to standard fluorescent DNA detection," *Biosens. Bioelectron.*, vol. 19, pp. 1149–1156, 2004.

[5] H. A. Ferreira, D. L. Graham, N. Feliciano, L. A. Clarke, M. D. Amaral, and P. P. Freitas, "Detection of cystic fibrosis related DNA targets using ac field focusing of magnetic labels and spin-valve sensors," *IEEE Trans. Magn.*, vol. 41, no. 10, pp. 4140–4142, Oct. 2005.

[6] L. Lagae, R. Wirix-Speetjens, C.-X. Liu, W. Laureyn, J. D. Boeck, G. Borghs, S. Harvey, P. Galvin, D. L. Graham, H. A. Ferreira, P. P. Freitas, L. A. Clarke, and M. D. Amaral, "Magnetic biosensors for genetic screening of cystic fibrosis," *Proc. IEE Circuits, Devices Syst.*, vol. 152, pp. 393–400, 2005.

[7] L. Ejsing, M. F. Hansen, A. K. Menon, H. A. Ferreira, D. L. Graham, and P. P. Freitas, "Planar Hall effect sensor for magnetic micro- and nanobead detection," *Appl. Phys. Lett.*, vol. 84, pp. 4729–4731, 2004.

[8] R. C. Sousa, P. P. Freitas, V. Chu, and J. P. Conde, "Vertical integration of a spin dependent tunnel junction with an amorphous Si diode for MRAM application," *IEEE Trans. Magn.*, vol. 35, no. 5, pp. 2832–2834, Sep. 1999.

[9] F. A. Cardoso, H. A. Ferreira, J. P. Conde, V. Chu, P. P. Freitas, D. Vidal, J. Germano, L. Sousa, M. S. Piedade, B. A. Costa, and J. M. Lemos, "Diode/MTJ cell for fully-scalable matrix-based biochip," *J. Appl. Phys.*, in press.

[10] M. Piedade, L. Sousa, J. Germano, J. Lemos, B. Costa, P. Freitas, H. Ferreira, F. Cardoso, and D. Vidal, "Architecture of a portable system based on a biochip for DNA recognition," in *Proc. XX Conf. Design of Circuits Integr. Syst.*, 2005.

[11] S. M. Sze, *Physics of Semiconductor Devices*, 2nd ed. New York: Wiley, 1981.

[12] *High Performance Digital Signal Controllers—dsPIC30F3010 DataSheets* (in Microchip), ref: DS70117E, 2005.

[13] *ARF32 Bluetooth Module Class 2* (in Adeunis R.F.), ref: 05–11–V5–pcy, 2003.

[14] *PIC18F2455/2550/4455/4550 Data Sheet* (in Microchip), ref: DS39632C, 2004.

[15] *Embedded Visual C++ 4.0* (in Microsoft), Part No. X03–71287, 2005.

Moisés Piedade received the Ph.D. degree in electrical and computer engineering from Instituto Superior Técnico (IST), Technical University of Lisbon, Lisbon, Portugal, in 1983.

He is a Professor in the Electrical and Computers Engineering Department, IST, and the Leader of SIPS Research Group at the Instituto de Engenharia de Sistemas e Computadores-R&D (INESC-ID), Lisbon, Portugal. His main research interests include electronic systems, signal acquisition and processing systems, and circuits and systems for biomedical applications.

Leonel Augusto Sousa (M'01–SM'03) received the Ph.D. degree in electrical and computer engineering from the Instituto Superior Técnico (IST), Technical University of Lisbon, Lisbon, Portugal, in 1996.

He is currently a faculty member in the Electrical and Computer Engineering Department, IST, and a Senior Researcher at Instituto de Engenharia de Sistemas e Computadores-R&D (INESC-ID), Lisbon, Portugal. His research interests include computer architectures, parallel and distributed computing, and VLSI architectures for multimedia and biomedical systems.

Teresa Mendes de Almeida received the diploma, M.Sc., and Ph.D. degrees in electrical and computer engineering from Instituto Superior Técnico (IST), Technical University of Lisbon, Lisbon, Portugal, in 1988, 1994, and 2005, respectively.

She is a Professor in the Electrical and Computers Engineering Department, IST and a Researcher at the Instituto de Engenharia de Sistemas e Computadores-R&D (INESC-ID), Lisbon, Portugal. Her research interests include analog and digital phase-locked loops, digital signal processing algorithms, and system modelling.

José Germano received the graduate degree in electrical and computer engineering and the M.Sc. degree from the Instituto Superior Técnico (IST), Technical University of Lisbon, Lisbon, Portugal, in 2004 and 2006, respectively. He is working toward the Ph.D. degree at the same institution.

His doctoral study focuses on the improvement of a data acquisition and processing platform for DNA recognition using a magnetoresistive biochip. His research interests include lab-on-chip, multimedia systems and processor micro-architectures.

Bertinho d'Andrade da Costa received the M.Sc. and Ph.D. degrees in electrical and computer engineering from the Instituto Superior Técnico (IST), Technical University of Lisbon, Lisbon, Portugal in 1992 and 1996, respectively.

He is currently a faculty member in the Electrical and Computer Engineering Department, IST, and a Researcher at Instituto de Engenharia de Sistemas e Computadores-R&D (INESC-ID), Lisbon, Portugal. His research interests include adaptive and predictive control, control applications, and computers for control.

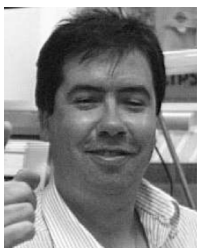

João Miranda Lemos received the Ph.D. degree in electrical and computer engineering from Instituto Superior Técnico (IST), Technical University of Lisbon, Lisbon, Portugal, in 1989, after extensive periods of work at the University of Florence, Florence, Italy.

He is a Professor in the Electrical and Computer Engineering Department, IST, and Leader of the Dynamic Systems Control Research Group at Instituto de Engenharia de Sistemas e Computadores-R&D (INESC-ID), Lisbon, Portugal. His main research interests include modelling and control of dynamic systems.

Paulo Peixeiro Freitas (M'90) received the Ph.D. degree in solid-state physics from Carnegie Mellon University, Pittsburgh, PA, in 1986.

He is now a Full Professor in the Physics Department of Instituto Superior Técnico (IST), Technical University of Lisbon, Lisbon, Portugal and the Director of Instituto de Engenharia de Sistemas e Computadores-Microsistemas & Nanotecnologias (INESC-MN), Lisbon, Portugal. His current research topics include MRAMS, read heads for ultra high-density recording, magnetoresistive biochips and bioelectronics, spin injection from transition metals into Si, and sensors.

Hugo A. Ferreira received the diploma degree in physics engineering from Instituto Superior Técnico (IST), Technical University of Lisbon, Lisbon, Portugal. He is working toward the Ph.D. degree at IST.

He is also working in magnetoresistive biochips at Instituto de Engenharia de Sistemas e Computadores-Microsistemas & Nanotecnologias (INESC-MN), Lisbon, Portugal.

Filipe Arroyo Cardoso received the diploma degree in physics engineering from Instituto Superior Técnico (IST), Technical University of Lisbon, Lisbon, Portugal. He is working toward the Ph.D. degree at IST.

He is also working in magnetoresistive biochips at Instituto de Engenharia de Sistemas e Computadores-Microsistemas & nanotecnologias (INESC-MN), Lisbon, Portugal.